Mathematics

Research article

Applied heat transfer modeling in conventional hybrid (Al₂O₃-CuO)/C₂H₆O₂ and modified-hybrid nanofluids (Al₂O₃-CuO-Fe₃O₄)/C₂H₆O₂ between slippery channel by using least square method (LSM)

Adnan[1,*], Khalid Abdulkhaliq M. Alharbi[2], Waqas Ashraf[3], Sayed M. Eldin[4], Mansour F. Yassen[5,6] and Wasim Jamshed[7]

[1] Department of Mathematics, Mohi-ud-Din Islamic University, Nerian Sharif 12080, AJ&K, Pakistan

[2] Mechanical Engineering Department, College of Engineering, Umm Al-Qura University, Makkah, 24382, Saudi Arabia

[3] Department of Applied Mathematics and Statistics (AM&S), Institute of Space Technology (IST), 44000 Islamabad, Pakistan

[4] Center of Research, Faculty of Engineering, Future University in Egypt, New Cairo 11835, Egypt

[5] Department of Mathematics, College of Science and Humanities in Al-Aflaj, Prince Sattam Bin Abdulaziz University, Al-Aflaj 11912, Saudi Arabia

[6] Department of Mathematics, Faculty of Science, Damietta University, New Damietta 34517 Damietta, Egypt

[7] Department of Mathematics, Capital University of Science and Technology, Islamabad, Pakistan

* Correspondence: Email: adnan_abbasi89@yahoo.com; Tel: +923315744284.

Abstract: In this research, a new heat transfer model for ternary nanofluid (Al₂O₃-CuO-Fe₃O₄)/C₂H₆O₂ inside slippery converging/diverging channel is reported with innovative effects of dissipation function. This flow situation described by a coupled set of PDEs which reduced to ODEs via similarity and effective ternary nanofluid properties. Then, LSM is successfully coded for the model and achieved the desired results influenced by α, Re, γ_1 and Ec. It is examined that the fluid movement increases for Re in the physical range of 30–180 and it drops for diverging channel ($\alpha > 0$) when the slippery wall approaches to $\alpha = 60^o$. The fluid movement is very slow for increasing

concentration factor ϕ_i for $i = 1,2,3$ up to 10%. Further, ternary nanofluid temperature boosts rapidly due to inclusion of trinanoparticles thermal conductivity and dissipation factor ($Ec = 0.1, 0.2, 0.3, 0.4, 0.6$) also contributes significantly. Moreover, the temperature is maximum about the center of the channel ($\eta = 0$) and slip effects ($\gamma_1 = 0.1, 0.2, 0.3, 0.4, 0.5, 0.6$) on the channel walls lead to decrement in the temperature $\beta(\eta)$.

Keywords: heat transfer; hybrid nanofluids; modified hybrid nanofluids; (Al_2O_3, CuO, Fe_3O_4) nanoparticles; converging/diverging channel; least square method
Mathematics Subject Classification: 76-11, 76D05

Abbreviations: PDEs: Partial differential equations; ODEs: Ordinary differential equations; LSM: Least Square Method

Nomenclature

$\breve{u}$	velocity component [m/s]
$\breve{p}$	pressure [Pa]
$\breve{T}$	temperature [K]
$\breve{U}$	velocity at central line [m/s]
$\breve{T}_w$	wall temperature [K]
$\tilde{\rho}_{mhnf}$	modified density [kgm^{-3}]
$\tilde{\rho}_{hnf}$	hybrid density [kgm^{-3}]
$\tilde{\rho}_f$	fluid density [kgm^{-3}]
$\tilde{\rho}_s$	nanoparticles density [kgm^{-3}]
$\tilde{\mu}_{mhnf}$	modified dynamic viscosity [Pa-s]
$\tilde{\mu}_{hnf}$	hybrid dynamic viscosity [Pa-s]
$\tilde{\mu}_f$	fluid dynamic viscosity [Pa-s]
$\breve{k}_{mhnf}$	modified thermal conductivity [Wm^{-1}K^{-1}]
$\breve{k}_{hnf}$	hybrid thermal conductivity [Wm^{-1}K^{-1}]
$\breve{k}_f$	fluid thermal conductivity [Wm^{-1}K^{-1}]
$\breve{k}_s$	nanoparticles thermal conductivity [Wm^{-1}K^{-1}]
$(\tilde{c}_p)_{mhnf}$	modified heat capacity [J/K]
$(\tilde{c}_p)_{hnf}$	hybrid heat capacity [J/K]
$(\tilde{c}_p)_f$	fluid heat capacity [J/K]
$(\tilde{c}_p)_s$	nanoparticles heat capacity [J/K]
η	dimensionless variable
F	dimensionless velocity
β	dimensionless temperature
ϕ	nanoparticles concentration
α	converging/diverging parameter
R_e	Reynolds number
Pr	Prandtl number

Ec Eckert number

γ_1 slip number

1. Introduction

The importance and applications of newtonian fluids (water, ethylene glycol, alcohol and glycerol etc.) cannot be avoided as the viscosity of these fluids remain unchanged under the action of forces and applicable in industries and engineering. As, interaction of oxide nanoparticles (Al_2O_3, CuO and Fe_3O_4) with common fluid in converging/diverging channel is important from the aspects of biomedical engineering which exhibits such flows. Therefore, an enhanced ternary nanofluid [1] model in converging/diverging is considered. The development of nanofluids made new insights in the modern world and engineers and researchers became familiar with these fluids. They feel that these fluids are very comfortable to overcome the issues of heat transport and can be used them in the production of various products.

The new type of heat transfer fluids synthesized using hybrid or ternary nanoparticles. Primarily, effective characteristics of these fluids are of much interest which are functions of diameter, temperature, concentration factor and brownian motion etc. Recently, Sahoo [2] performed an experiment and introduced a new viscosity model for ternary nanofluid. The experiment executed for (Al_2O_3-SiC-TiO_2)/water with uniform dispersion of each type of nanoparticles within 35–40 °C temperature. In 2021, Zayan et al. [3] discussed rheological properties of (GO-TiO_2-Ag)/H_2O and (TiO_2-Ag-rGO)/H_2O via experiment. They examined that simple GO based trinanoparticles under temperature variations from 25–50 °C exhibit newtonian characteristics. However, at low concentration it behaves like Pseudo Plastic and major contribution of nanoparticles aggregation is suggested to acquire the goal. Numerical treatment of fluid with basic components of trinanoparticles including the nonuniform diffusion and non-Fourier heat flux reported by Algehyne et al. [4]. The authors examined that the hybrid nanoliquid has larger tendency to transmit and store energy and it boosts almost 61% to that of mono nanoliquid.

Recently, Dezfulizadeh et al. [5] proposed an effective correlation to improve the heat transfer capacity of ternary fluids. They inspired by thermomechanical characteristics of (Cu-SiO_2-MWCNT) and reported the correlations. After the development of variety of effective characteristics of ternary nanoliquids under different circumstances, researchers from applied areas inspired and analyze them from more advanced physical aspects [6]. Further, recent advancements in ternary nanofluids for nanomaterials owing to their outstanding thermal and mechanical characteristics described in the Refs. [7,8] and the studies reported therein.

Nanofluids synthesized from uniform composition of nano-additives in the hosting liquid. The dimensions of nanoparticles are usually smaller than 100nm which allow them to dissolve in the base solvent uniformly. The progressive thermal conductivity of nanofluids attracts the attention of industrialist, engineers and scientists for wide applications. These broadly applicable in thermal engineering, heat transport problems, bio-medical engineering [9], pollution control and building heating/cooling, heat enhancement [10], electronics, paint industries and aerodynamics etc. Interaction of nanoparticles with blood as base liquid became very innovative in the medical sciences, more specifically for detection of cancer cells in human body [11,12]. So that, the world entered into a new era with broad and innovative ideas. The composition process of nanofluids is sketched in Figure 1.
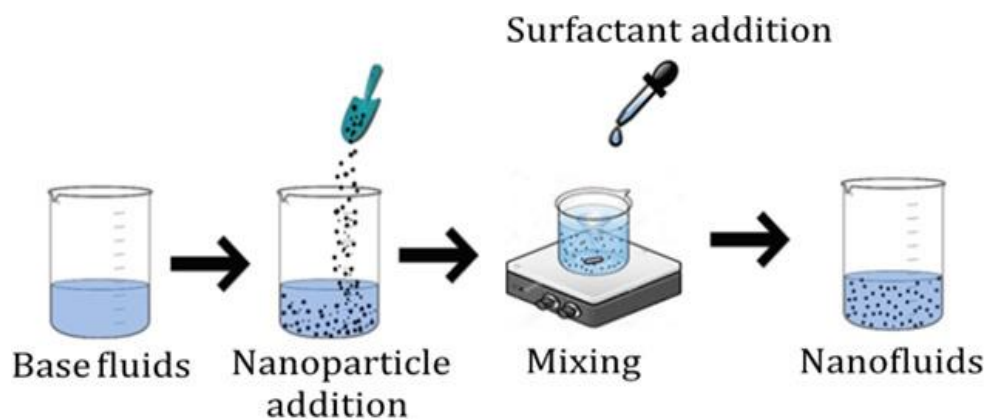
Figure 1. Synthesization capturing of nanofluids (first generation heat transfer fluids).

After the primary idea of nanofluids, researchers became very curious and invested time to make these fluids effective regarding thermal performance. They thought that inherent characteristics of conventional liquids could be enhanced by adding one more sort of nanoparticles. So, they worked day and night and finally they succeeded and achieve a milestone of Hybrid nanofluids [13,14]. These fluids known as second-generation heat transfer fluids with rich thermal conductivity. Recently, researchers reveal that hybrid nanofluids have promising heat transport characteristics due to which these substitute the conventional fluids. These fluids have broad range of applications in the world of nanotechnology, some of them are in solar collectors, solar energy storage devices, cooling parts of electronic devices, manufacturing of various machinery parts, air conditioning, ventilation, heat exchangers and refrigeration etc. The schematic of synthetization of hybrid nanoliquids is demonstrated in Figure 2.
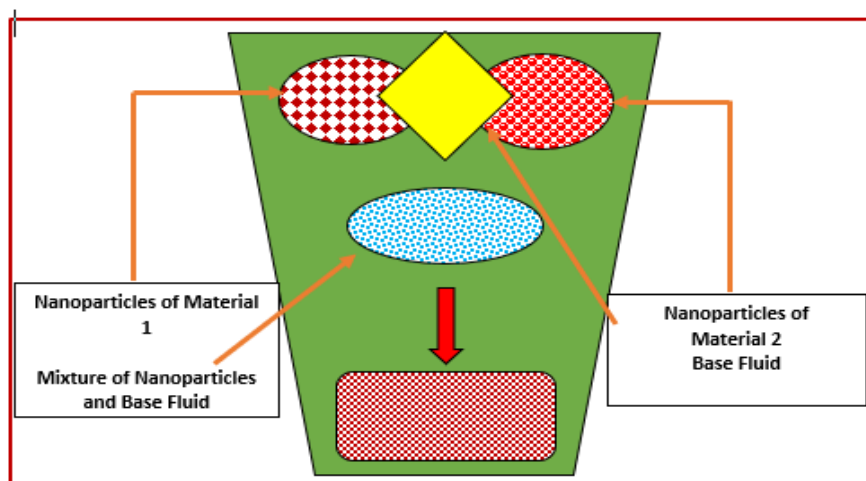

Figure 2. Synthesization capturing of Hybrid nanofluids (Second generation heat transfer fluids).

Although, hybrid nanofluids have promising applications in the world of nanotechnology; however, scientists did not stop their efforts to resolve the challenges that could be found in engineering and industrial zone. Therefore, leading scientists of the world gathered at a single platform and revealed that promising heat transport characteristics of hybrid nanofluids could be improved further by adding

a third type nanoparticles in the existing hybrid nanofluids. Finally, they introduced the modern world with the concept of Ternary-hybrid nanofluids [15–18]. The addition of third type of nanoparticles in the regular hybrid nanofluids boosts thermal conductivity of the resultant mixture that makes them superior heat transport fluids.

In the view of above discussion and literature cited, the following classes exist so far to tackle the heat transport issues of the modern world:

- Conventional fluids with inherent characteristics (poor conductor of heat transport).
- Nanofluids or first-generation heat transfer fluids (better thermal performance than conventional liquids).
- Hybrid nanofluids or second-generation heat transfer fluids (superior thermal performance than conventional and nanofluids).
- Ternary hybrid nanofluids or third-generation heat transfer fluids (recently developed heat transfer fluids with excellent thermal transport characteristics than regular, nanofluids and hybrid nanofluids).

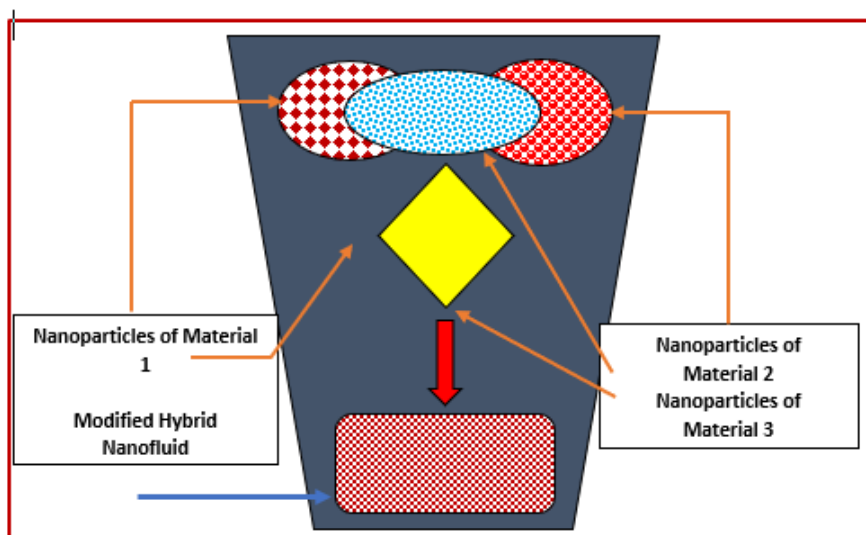Figure 3 illustrated synthetization process of tri-hybrid nanofluids.

Figure 3. Synthesization capturing of Tri-Hybrid nanofluids (Third generation heat transfer fluids).

The rapid growth in the study of heat transport problems provided a new ground to Fluid dynamists to explore the interaction of various flow conditions and physical phenomenon with varying nanomaterials. The production process of industrial products passes through many stages in which the fluid flow through different geometries. In the language of Fluid mechanics, these flow situations modeled through constitutive relations that are latterly used to examine the impacts of physical constraints. For example, magnetic field [19] and Joule heating phenomenon could be utilized to purify the industrial production or thermal radiations [20] effects, velocity and thermal slip constraints, heat generation/absorption [21], activation energy or cross diffusion gradients are such physical constraints that playing imperative role in the modern world.

The detection of different health related diseases is a core issue around the globe and oxide nanoparticles (Al_2O_3, CuO, Fe_3O_4) are widely utilize to cope the problems of implant, wound healing,

cancer therapy, antimicrobial activities, drug delivery and in bio-medical sciences [22]. Therefore, in the view of above discussed significant aspects of oxide nanoparticles, this study is organized and it will cover the following research gaps:

- Comparative thermal behaviour between [(Al$_2$O$_3$-CuO)/C$_2$H$_6$O$_2$]$_{hnf}$ and ternary hybrid nanofluid [(Al$_2$O$_3$-CuO-Fe$_3$O$_4$)/C$_2$H$_6$O$_2$]$_{mhnf}$.
- The insertion of viscous dissipation in the model strengthens the novelty of the research in the context of thermal enhancement.
- Impacts of fraction factor ϕ of (Al$_2$O$_3$, CuO, Fe$_3$O$_4$) will be examined.
- The quantities of engineering concerns like skin friction coefficient will be examined by fluctuating the physical constraints.
- The models for [(Al$_2$O$_3$-CuO)/C$_2$H$_6$O$_2$]$_{hnf}$ and ternary hybrid nanofluid [(Al$_2$O$_3$-CuO-Fe$_3$O$_4$)/C$_2$H$_6$O$_2$]$_{mhnf}$ will be solved by utilizing Least Square Method (LSM).

2. Materials and methods

2.1. Development of the model

In this analysis, considered the steady, incompressible, 2D but unidirectional flow of [(Al$_2$O$_3$-CuO)/C$_2$H$_6$O$_2$]$_{hnf}$ and [(Al$_2$O$_3$-CuO-Fe$_3$O$_4$)/C$_2$H$_6$O$_2$]$_{mhnf}$ nanofluids inspired by the novel effects of viscous dissipation and thermal radiation. The fluids flow due a source/sink positioned at the culmination point of the slippery walls in the polar frame. The walls of the channel are separated through separation angle 2α and the flow is only along radial direction. Due to unidirectional flow configuration, the fluid accelerates because of only $\breve{u}$ velocity component. Thus, possible velocity vector takes the form $\boldsymbol{V} = (\breve{u}, 0,0)$ in which $\breve{u}$ depends on polar coordinates r and θ. The physical scenario of the flow is pictured in Figure 4. Moreover, in the light of aforesaid conditions, three basic laws are then described the following mathematical expressions [23]:

$$\frac{1}{r}(r\breve{u})_r = 0 \tag{1}$$

$$\tilde{\rho}_{mhnf}[\breve{u}\breve{u}_r] + [\breve{p}]_r - \tilde{\mu}_{mhnf}\left[\breve{u}_{rr} + \frac{1}{r}\breve{u}_r + \frac{1}{r^2}\breve{u}_{\theta\theta} - \frac{\breve{u}}{r^2}\right] = 0 \tag{2}$$

$$-\frac{1}{r\tilde{\rho}_{mhnf}}[\breve{p}]_\theta + \frac{2\tilde{\mu}_{mhnf}}{\tilde{\rho}_{mhnf}r^2}[\breve{u}]_\theta = 0 \tag{3}$$

$$\breve{u}[\breve{T}]_r - \frac{\breve{k}_{mhnf}}{(\tilde{\rho}Cp)_{mhnf}}\left[\breve{T}_{rr} + \frac{1}{r}\breve{T}_r + \frac{1}{r^2}\breve{T}_{\theta\theta}\right] - \tilde{\mu}_{\frac{mhnf}{(\tilde{\rho}Cp)_{mhnf}}}\left[4(\breve{u})_r^2 + \frac{1}{r^2}(\breve{u})_\theta^2\right] = 0 \tag{4}$$

Here, subscripts r and θ represent the differentiation w.r.t polar coordinates, $mhnf$ stands for modified hybrid nanofluid, $\tilde{\rho}_{mhnf}$, $\tilde{\mu}_{mhnf}$, $\breve{k}_{mhnf}$ $(\tilde{\rho}Cp)_{mhnf}$ are effective density, dynamic viscosity, thermal conductance and heat capacitance of modified hybrid nanofluid. The flow of [(Al$_2$O$_3$-CuO)/C$_2$H$_6$O$_2$]$_{hnf}$ and [(Al$_2$O$_3$-CuO-Fe$_3$O$_4$)/C$_2$H$_6$O$_2$]$_{mhnf}$ confined to the following conditions [23]:

$$\breve{u} = \breve{U}, \breve{u}_\theta = 0, \breve{T}_\theta = 0 \quad \text{at } \theta = 0 \tag{5}$$

$$\breve{u} = -\gamma_1\breve{u}_\theta, \breve{T} = \breve{T}_w \quad \text{at } \theta = \alpha \tag{6}$$
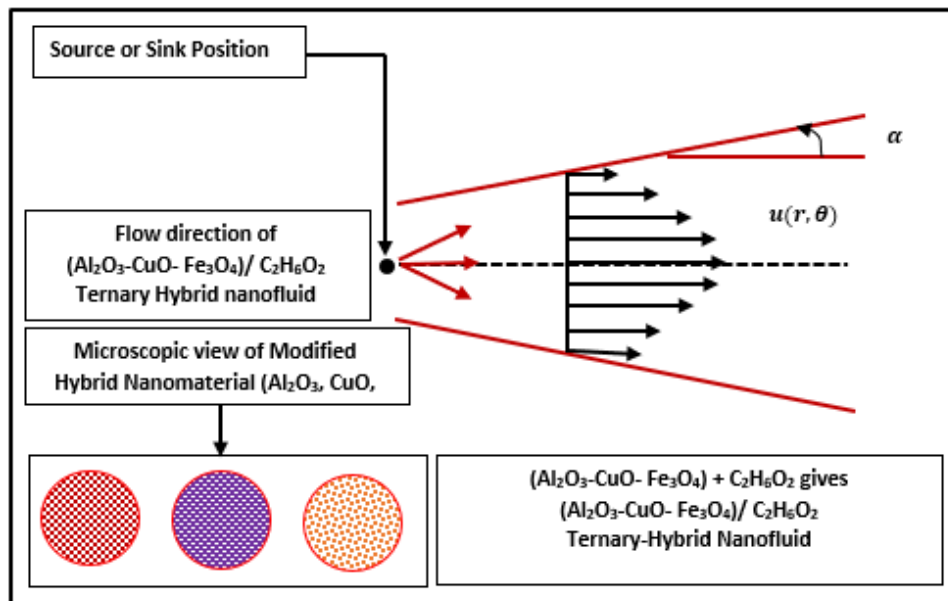
Figure 4. Flow configuration of [Al$_2$O$_3$-CuO/C$_2$H$_6$O$_2$]$_{hnf}$ and [Al$_2$O$_3$-CuO-Fe$_3$O$_4$/C$_2$H$_6$O$_2$]$_{mhnf}$ between converging/diverging channel.

Physically, these conditions describe that the fluid particles move with maximum speed at the central line i.e., $\theta = 0$ and temperature is $\check{T}_\theta$. On the other hand, slip condition is implemented at the walls ($\theta = \alpha$) and the temperature of fluid layer adjacent to the wall is same as the wall temperature $\check{T}_w$.

Now, Eq (1) can be transformed in the following version on integrating and also supporting similarity expression as described [23]:

$$F(\eta) = \frac{\check{f}(\theta)}{\check{f}_{max}}, \eta = \theta\alpha^{-1}, \beta(\eta) = \frac{\check{T}}{\check{T}_w}$$

The following empirical correlations are adopted to update the conventional nanofluid models for hybrid and ternary hybrid nanofluids (THNF) (See Tables 1–3, [24–26]).

Table 1. Empirical attributes of nanofluids.

Characteristics	Empirical attributes
Dynamic viscosity	$\dfrac{\tilde{\mu}_{nf}}{\tilde{\mu}_f} = (1-\phi)^{-25/10}$
Effective density	$\tilde{\rho}_{nf} = \tilde{\rho}_f(1-\phi) + \tilde{\rho}_s\phi$
Heat capacity	$(\tilde{\rho}C_p)_{nf} = (\tilde{\rho}C_p)_f(1-\phi) + \phi(\tilde{\rho}C_p)_s$
Thermal conductivity	$\dfrac{\check{k}_{nf}}{\check{k}_f} = \dfrac{[\check{k}_s + \check{k}_f(\tilde{\chi}-1) - (\tilde{\chi}-1)(\check{k}_f - \check{k}_s)\phi]}{[\check{k}_s + \check{k}_f(\tilde{\chi}-1) + (\check{k}_f - \check{k}_s)\phi]}$ where, $\tilde{\chi} = \dfrac{3}{\tilde{\Phi}}$ is the shape factor
Electrical conductivity	$\dfrac{\tilde{\sigma}_{nf}}{\tilde{\sigma}_f} = 1 + \dfrac{3\left(\frac{\tilde{\sigma}_s}{\tilde{\sigma}_f}-1\right)\phi}{\left(\frac{\tilde{\sigma}_s}{\tilde{\sigma}_f}+2\right) - \left(\frac{\tilde{\sigma}_s}{\tilde{\sigma}_f}-1\right)\phi}$
Thermal expansion	$(\rho\beta)_{nf} = (1-\phi)(\rho\beta)_s + \phi(\rho\beta)_f$

Table 2. Empirical attributes for hybrid nanofluids [27].

Characteristics	Empirical attributes
Dynamic viscosity	$\dfrac{\tilde{\mu}_{hnf}}{\tilde{\mu}_f} = (1-\phi_1)^{-25/10}(1-\phi_2)^{-25/10}$
Effective density	$\tilde{\rho}_{hnf} = \left[(1-\phi_2)\{(1-\phi_1)\tilde{\rho}_f + \phi_1\tilde{\rho}_{s1}\}\right] + \phi_2\tilde{\rho}_{s2}$
Heat capacity	$(\tilde{\rho}C_p)_{hnf} = \left[(1-\phi_2)\left\{(1-\phi_1)(\tilde{\rho}C_p)_f + \phi_1(\tilde{\rho}C_p)_{s1}\right\}\right] +$ $\phi_2(\tilde{\rho}C_p)_{s2}$
Thermal conductivity	$\dfrac{\check{k}_{hnf}}{\check{k}_{nf}} = \dfrac{[\check{k}_{s2} + (\tilde{\chi}-1)\check{k}_{nf} - (\tilde{\chi}-1)\phi_2(\check{k}_{nf} - \check{k}_{s2})]}{[\check{k}_{s2} + (\tilde{\chi}-1)\check{k}_{nf} + \phi_2(\check{k}_{nf} - \check{k}_{s2})]}$ where $\dfrac{\check{k}_{nf}}{\check{k}_f} = \dfrac{[\check{k}_{s1} + \check{k}_f(\tilde{\chi}-1) - (\tilde{\chi}-1)(\check{k}_f - \check{k}_{s1})\phi_1]}{[\check{k}_{s1} + \check{k}_f(\tilde{\chi}-1) + (\check{k}_f - \check{k}_{s1})\phi_1]}$
Electrical conductivity	$\dfrac{\tilde{\sigma}_{hnf}}{\tilde{\sigma}_{nf}} = \dfrac{[\tilde{\sigma}_{s2} + 2\tilde{\sigma}_{nf} - 2\phi_2(\tilde{\sigma}_{nf} - \tilde{\sigma}_{s2})]}{[\tilde{\sigma}_{s2} + 2\tilde{\sigma}_{nf} + \phi_2(\tilde{\sigma}_{nf} - \tilde{\sigma}_{s2})]}$ where $\dfrac{\tilde{\sigma}_{nf}}{\tilde{\sigma}_f} = \dfrac{[\tilde{\sigma}_{s1} + 2\tilde{\sigma}_f - 2\phi_1(\tilde{\sigma}_f - \tilde{\sigma}_{s1})]}{[\tilde{\sigma}_{s1} + 2\tilde{\sigma}_f + \phi_1(\tilde{\sigma}_f - \tilde{\sigma}_{s1})]}$
Thermal expansion	$(\tilde{\rho}\tilde{\beta})_{nf} = \left[(1-\phi_2)\left\{(1-\phi_1)(\tilde{\rho}\tilde{\beta})_f + \phi_1(\tilde{\rho}\tilde{\beta})_{s1}\right\}\right] + \phi_2(\tilde{\rho}\tilde{\beta})_{s2}$

Table 3. Empirical attributes of ternary hybrid nanofluids.

Characteristics	Empirical attributes
Dynamic viscosity	$\dfrac{\tilde{\mu}_{mhnf}}{\tilde{\mu}_f} = (1-\phi_1)^{-25/10}(1-\phi_2)^{-25/10}(1-\phi_3)^{-25/10}$
Effective density	$\tilde{\rho}_{mhnf} = \left[(1-\phi_3)\{(1-\phi_2)[(1-\phi_1)\tilde{\rho}_f + \phi_1\tilde{\rho}_{s1}] + \phi_2\tilde{\rho}_{s2}\}\right] + \phi_3\tilde{\rho}_{s3}$
Heat capacity	$(\tilde{\rho}C_p)_{mhnf} = \Big[(1-\phi_3)\Big\{(1-\phi_2)\Big[(1-\phi_1)(\tilde{\rho}C_p)_f + \phi_1(\tilde{\rho}C_p)_{s1}\Big] +$ $\phi_2(\tilde{\rho}C_p)_{s2}\Big\}\Big] + \phi_3(\tilde{\rho}C_p)_{s3}$
Thermal conductivity	$\dfrac{\tilde{k}_{mhnf}}{\tilde{k}_{hnf}} = \dfrac{[\tilde{k}_{s3}+(\tilde{\chi}-1)\tilde{k}_{hnf}-(\tilde{\chi}-1)\phi_3(\tilde{k}_{hnf}-\tilde{k}_{s3})]}{[\tilde{k}_{s3}+(\tilde{\chi}-1)\tilde{k}_{hnf}+\phi_3(\tilde{k}_{hnf}-\tilde{k}_{s3})]}$ where $\dfrac{\tilde{k}_{hnf}}{\tilde{k}_{nf}} = \dfrac{[\tilde{k}_{s2}+(\tilde{\chi}-1)\tilde{k}_{nf}-(\tilde{\chi}-1)\phi_2(\tilde{k}_{nf}-\tilde{k}_{s2})]}{[\tilde{k}_{s2}+(\tilde{\chi}-1)\tilde{k}_{nf}+\phi_2(\tilde{k}_{nf}-\tilde{k}_{s2})]}$ where $\dfrac{\tilde{k}_{nf}}{\tilde{k}_f} = \dfrac{[\tilde{k}_{s1}+(\tilde{\chi}-1)\tilde{k}_f-(\tilde{\chi}-1)\phi_1(\tilde{k}_f-\tilde{k}_{s1})]}{[\tilde{k}_{s1}+(\tilde{\chi}-1)\tilde{k}_f+\phi_1(\tilde{k}_f-\tilde{k}_{s1})]}$
Electrical conductivity	$\dfrac{\tilde{\sigma}_{mhnf}}{\tilde{\sigma}hn_f} = \dfrac{[\tilde{\sigma}_{s3}+2\tilde{\sigma}_{hnf}-2\phi_3(\tilde{\sigma}_{hnf}-\tilde{\sigma}_{s3})]}{[\tilde{\sigma}_{s3}+2\tilde{\sigma}_{hnf}+\phi_3(\tilde{\sigma}_{hnf}-\tilde{\sigma}_{s3})]}$ where $\dfrac{\tilde{\sigma}_{hnf}}{\tilde{\sigma}n_f} = \dfrac{[\tilde{\sigma}_{s2}+2\tilde{\sigma}_{nf}-2\phi_2(\tilde{\sigma}_{nf}-\tilde{\sigma}_{s2})]}{[\tilde{\sigma}_{s2}+2\tilde{\sigma}_{nf}+\phi_2(\tilde{\sigma}_{nf}-\tilde{\sigma}_{s2})]}$ where $\dfrac{\tilde{\sigma}_{nf}}{\tilde{\sigma}_f} = \dfrac{[\tilde{\sigma}_{s1}+2\tilde{\sigma}_f-2\phi_1(\tilde{\sigma}_f-\tilde{\sigma}_{s1})]}{[\tilde{\sigma}_{s1}+2\tilde{\sigma}_f+\phi_1(\tilde{\sigma}_f-\tilde{\sigma}_{s1})]}$

Table 4. Nanoparticles name, shapes and shape factor values.

Nanoparticle's name	Shape	Shape factor $\tilde{\chi}$
Lamina		16.1576
Platelets		5.7
Hexahedron		3.7221

Further, shape factor of the nanoparticles is defined in Table 4 for different sort of nanoparticles [28].

Now, after performing necessary cross differentiation of the momentum equations and impinging the similarity equations and empirical correlations, the following updating version of the model is obtained:

$$F_{\eta\eta} + \frac{2\alpha Re\left[\left[(1-\phi_3)\left\{(1-\phi_2)\left[(1-\phi_1)+\frac{\phi_1\tilde{\rho}_{s1}}{\tilde{\rho}_f}\right]+\frac{\phi_2\tilde{\rho}_{s2}}{\tilde{\rho}_f}\right\}\right]+\frac{\phi_3\tilde{\rho}_{s3}}{\tilde{\rho}_f}\right]}{(1-\phi_1)^{-25/10}(1-\phi_2)^{-25/10}(1-\phi_3)^{-25/10}}FF_{\eta} + 4\alpha^2 F_{\eta} = 0 \tag{7}$$

$$\frac{\tilde{k}_{mhnf}}{\tilde{k}_f}\beta_{\eta\eta} + \frac{EcPr\left[\left[(1-\phi_3)\left\{(1-\phi_2)\left[(1-\phi_1)+\frac{\phi_1(\tilde{\rho}c_p)_{s1}}{(\tilde{\rho}c_p)_f}\right]+\frac{\phi_2(\tilde{\rho}c_p)_{s2}}{(\tilde{\rho}c_p)_f}\right\}\right]+\frac{\phi_3(\tilde{\rho}c_p)_{s3}}{(\tilde{\rho}c_p)_f}\right]}{(1-\phi_1)^{\frac{25}{10}}(1-\phi_2)^{\frac{25}{10}}(1-\phi_3)^{\frac{25}{10}}}\left(4\alpha^2 F^2 + F_{\eta}^2\right) = 0 \tag{8}$$

$$\frac{\tilde{k}_{mhnf}}{\tilde{k}_f} = \frac{\left[\tilde{k}_{s3} + (\tilde{\chi}-1)\tilde{k}_{hnf} - (\tilde{\chi}-1)\phi_3\left(\tilde{k}_{hnf} - \tilde{k}_{s3}\right)\right]}{\left[\tilde{k}_{s3} + (\tilde{\chi}-1)\tilde{k}_{hnf} + \phi_3\left(\tilde{k}_{hnf} - \tilde{k}_{s3}\right)\right]}$$

$$* \frac{\left[\tilde{k}_{s2} + (\tilde{\chi}-1)\tilde{k}_{nf} - (\tilde{\chi}-1)\phi_2\left(\tilde{k}_{nf} - \tilde{k}_{s2}\right)\right]}{\left[\tilde{k}_{s2} + (\tilde{\chi}-1)\tilde{k}_{nf} + \phi_2\left(\tilde{k}_{nf} - \tilde{k}_{s2}\right)\right]}$$

$$* \frac{\left[\tilde{k}_{s1} + (\tilde{\chi}-1)\tilde{k}_f - (\tilde{\chi}-1)\phi_1\left(\tilde{k}_f - \tilde{k}_{s1}\right)\right]}{\left[\tilde{k}_{s1} + (\tilde{\chi}-1)\tilde{k}_f + \phi_1\left(\tilde{k}_f - \tilde{k}_{s1}\right)\right]}$$

The functions F and β depend on η. Similarly, the boundary conditions (BCs) transformed in the following version:

$$F(\eta) = 1, F'(\eta) = 0, \beta'(\eta) = 0 \text{ at } \eta = 0$$

$$F(\eta) = -\gamma_1 F'(\eta), \beta(\eta) = 0 \text{ at } \eta = 1$$

The quantity of broad engineering interest (Skin friction coefficient) is modeled in the following way:

$$\check{C}_F = \frac{\tilde{\mu}_{mhnf}}{\tilde{U}^2\tilde{\rho}_{mhnf}}[\tilde{\tau}_{r\theta}]_{\eta=1}$$

By adopting the shear stresses and empirical correlations, the following form is attained after performing some mathematical steps:

$$Re_r\tilde{C}_F = \frac{F'(\eta)_{\eta=1}}{\left[(1-\phi_1)^{\frac{25}{10}}(1-\phi_2)^{\frac{25}{10}}(1-\phi_3)^{\frac{25}{10}}\right]*\left[\left[(1-\phi_3)\left\{(1-\phi_2)\left[(1-\phi_1)+\frac{\phi_1\tilde{\rho}_{s1}}{\tilde{\rho}_f}\right]+\frac{\phi_2\tilde{\rho}_{s2}}{\tilde{\rho}_f}\right\}\right]+\frac{\phi_3\tilde{\rho}_{s3}}{\tilde{\rho}_f}\right]} \tag{9}$$

The physical constraints appeared in the above model are Eckert number ($Ec = \frac{\tilde{\mu}_f(c_p)_f}{\tilde{k}_f}$) and velocity slip ($\gamma_1 = \frac{\gamma}{\alpha}$). Moreover, thermophysical values for aforementioned empirical correlations are described in Table 5.

Table 5. Thermophysical values of the guest nanoparticles and the host liquid.

Properties	$\hat{\rho}(kg/m^3)$	$\hat{c}_p(J/Kg\ K)$	$\hat{k}(W/mk)$	$\breve{\sigma}(\Omega m)^{-1}$
Ethylene glycol ($C_2H_6O_2$)	1115	2430	0.253	---------
Al_2O_3	3970	765	40	35×10^6
Cu	8933	385	400	59.6×10^6
CuO	6500	540	18	6.9×10^{-2}
Fe_3O_4	5180	670	9.7	0.74×10^6

2.2. Mathematical analysis

The solution of the model described in Eqs (7) and (8) alongside BCs is achieved via Least Square Method (LSM). The LSM works according to the following procedure:

2.2.1. Step 1

In this step, consider the model that going to be solved by LSM. Thus, the following enhanced heat transfer flow model is taken:

$$F_{\eta\eta\eta} + \frac{2\alpha Re\left[\left[(1-\phi_3)\left\{(1-\phi_2)\left[(1-\phi_1)+\frac{\phi_1\tilde{\rho}_{s1}}{\tilde{\rho}_f}\right]+\frac{\phi_2\tilde{\rho}_{s2}}{\tilde{\rho}_f}\right\}\right]+\frac{\phi_3\tilde{\rho}_{s3}}{\tilde{\rho}_f}\right]}{(1-\phi_1)^{-25/10}(1-\phi_2)^{-25/10}(1-\phi_3)^{-25/10}} FF_{\eta} + 4\alpha^2 F_{\eta} = 0 \tag{10}$$

$$\frac{\tilde{k}_{mhnf}}{\tilde{k}_f}\beta_{\eta\eta} + \frac{EcPr\left[\left[(1-\phi_3)\left\{(1-\phi_2)\left[(1-\phi_1)+\frac{\phi_1(\tilde{\rho}c_p)_{s1}}{(\tilde{\rho}c_p)_f}\right]+\frac{\phi_2(\tilde{\rho}c_p)_{s2}}{(\tilde{\rho}c_p)_f}\right\}\right]+\frac{\phi_3(\tilde{\rho}c_p)_{s3}}{(\tilde{\rho}c_p)_f}\right]}{(1-\phi_1)^{\frac{25}{10}}(1-\phi_2)^{\frac{25}{10}}(1-\phi_3)^{\frac{25}{10}}}\left(4\alpha^2 F^2 + F_{\eta}^2\right) = 0 \tag{11}$$

$$\frac{\tilde{k}_{mhnf}}{\tilde{k}_f} = \frac{\left[\tilde{k}_{s3} + (\tilde{\chi}-1)\tilde{k}_{hnf} - (\tilde{\chi}-1)\phi_3\left(\tilde{k}_{hnf} - \tilde{k}_{s3}\right)\right]}{\left[\tilde{k}_{s3} + (\tilde{\chi}-1)\tilde{k}_{hnf} + \phi_3\left(\tilde{k}_{hnf} - \tilde{k}_{s3}\right)\right]}$$

$$* \frac{\left[\tilde{k}_{s2} + (\tilde{\chi}-1)\tilde{k}_{nf} - (\tilde{\chi}-1)\phi_2\left(\tilde{k}_{nf} - \tilde{k}_{s2}\right)\right]}{\left[\tilde{k}_{s2} + (\tilde{\chi}-1)\tilde{k}_{nf} + \phi_2\left(\tilde{k}_{nf} - \tilde{k}_{s2}\right)\right]}$$

$$* \frac{\left[\tilde{k}_{s1} + (\tilde{\chi}-1)\tilde{k}_f - (\tilde{\chi}-1)\phi_1\left(\tilde{k}_f - \tilde{k}_{s1}\right)\right]}{\left[\tilde{k}_{s1} + (\tilde{\chi}-1)\tilde{k}_f + \phi_1\left(\tilde{k}_f - \tilde{k}_{s1}\right)\right]}$$

2.2.2. Step 2

In this step, trial solutions of the model equations defined in the following way:

$$\breve{F} = \mathfrak{I}_0 + \mathfrak{I}_1\eta + \mathfrak{I}_2\eta^2 + \mathfrak{I}_3\eta^3 + \mathfrak{I}_4\eta^4 + \cdots + \mathfrak{I}_n\eta^n = \sum_{l=0}^{n} \mathfrak{I}_l\eta^l$$

$$\check{\beta} = \widetilde{\widetilde{\mathfrak{I}}}_0 + \widetilde{\widetilde{\mathfrak{I}}}_1 \eta + \widetilde{\widetilde{\mathfrak{I}}}_2 \eta^2 + \widetilde{\widetilde{\mathfrak{I}}}_3 \eta^3 + \widetilde{\widetilde{\mathfrak{I}}}_4 \eta^4 + \cdots + \widetilde{\widetilde{\mathfrak{I}}}_n \eta^n = \sum_{l=0}^{n} \widetilde{\widetilde{\mathfrak{I}}}_l \eta^l$$

In these expressions, $\check{F}$ and $\check{\beta}$ depend on the variable η. The proposed trial solutions must gratify the BCs of the flow model.

2.2.3. Step 3

By means of trial solutions, residual vectors for the governing flow model [(Al$_2$O$_3$-CuO-Fe$_3$O$_4$)/C$_2$H$_6$O$_2$]$_{mhnf}$ in Eqs (10) and (11) described in the following way:

$$\boldsymbol{R}_F = \check{F}_{\eta\eta} + \frac{2\alpha Re\left[\left[(1-\phi_3)\left\{(1-\phi_2)\left[(1-\phi_1)+\frac{\phi_1 \check{\rho}_{s1}}{\check{\rho}_f}\right]+\frac{\phi_2 \check{\rho}_{s2}}{\check{\rho}_f}\right\}\right]+\frac{\phi_3 \check{\rho}_{s3}}{\check{\rho}_f}\right]}{(1-\phi_1)^{-25/10}(1-\phi_2)^{-25/10}(1-\phi_3)^{-25/10}} \check{F}\check{F}_\eta + 4\alpha^2 \check{F}_\eta \cong 0$$

$$\boldsymbol{R}_\beta = \frac{\tilde{k}_{mhnf}}{\tilde{k}_f}\check{\beta}_{\eta\eta} + \frac{EcPr\left[\left[(1-\phi_3)\left\{(1-\phi_2)\left[(1-\phi_1)+\frac{\phi_1 (\check{\rho}c_p)_{s1}}{(\check{\rho}c_p)_f}\right]+\frac{\phi_2 (\check{\rho}c_p)_{s2}}{(\check{\rho}c_p)_f}\right\}\right]+\frac{\phi_3 (\check{\rho}c_p)_{s3}}{(\check{\rho}c_p)_f}\right]}{(1-\phi_1)^{\frac{25}{10}}(1-\phi_2)^{\frac{25}{10}}(1-\phi_3)^{\frac{25}{10}}} \left(4\alpha^2 \check{F}^2 + \check{F}_\eta^2\right) \cong 0$$

$$\frac{\tilde{k}_{mhnf}}{\tilde{k}_f} = \frac{\left[\tilde{k}_{s3} + (\tilde{\chi}-1)\tilde{k}_{hnf} - (\tilde{\chi}-1)\phi_3\left(\tilde{k}_{hnf} - \tilde{k}_{s3}\right)\right]}{\left[\tilde{k}_{s3} + (\tilde{\chi}-1)\tilde{k}_{hnf} + \phi_3\left(\tilde{k}_{hnf} - \tilde{k}_{s3}\right)\right]} * \frac{\left[\tilde{k}_{s2} + (\tilde{\chi}-1)\tilde{k}_{nf} - (\tilde{\chi}-1)\phi_2\left(\tilde{k}_{nf} - \tilde{k}_{s2}\right)\right]}{\left[\tilde{k}_{s2} + (\tilde{\chi}-1)\tilde{k}_{nf} + \phi_2\left(\tilde{k}_{nf} - \tilde{k}_{s2}\right)\right]}$$
$$* \frac{\left[\tilde{k}_{s1} + (\tilde{\chi}-1)\tilde{k}_f - (\tilde{\chi}-1)\phi_1\left(\tilde{k}_f - \tilde{k}_{s1}\right)\right]}{\left[\tilde{k}_{s1} + (\tilde{\chi}-1)\tilde{k}_f + \phi_1\left(\tilde{k}_f - \tilde{k}_{s1}\right)\right]}$$

2.2.4. Step 4

From hereafter, we need to construct a system of algebraic equations with equal number of unknowns as that of equations. In LSM, the following idea is utilized to construct the desired systems of equations:

$$\boldsymbol{E}_F = \int \boldsymbol{R}_F(\eta)\widetilde{\omega}^F{}_l d\eta = 0, \quad l = 0,1,2,3,\ldots n$$

$$\boldsymbol{E}_\beta = \int \boldsymbol{R}_\beta(\eta)\widetilde{\omega}^\beta{}_l d\eta = 0, \quad l = 0,1,2,3,\ldots n$$

In these constructive relations, $\widetilde{\omega}^F{}_l$ and $\widetilde{\omega}^\beta{}_l$ are the weight functions for F and β, respectively. These weight function achieved by implementing the following weight functions formula:

$$\widetilde{\omega}^F{}_l = \frac{\partial \boldsymbol{R}_F}{\partial \widetilde{\mathfrak{I}}_n}, \qquad \widetilde{\omega}^\beta{}_l = \frac{\partial \boldsymbol{R}_\beta}{\partial \widetilde{\widetilde{\mathfrak{I}}}_n}$$

2.2.5. Step 5

By using the system of algebraic equations in the preceding step, $\widetilde{\mathfrak{I}}'s$ values computed and then plugging all the values in trial solutions, final solution of the original system will be achieved.

3. Results and discussion

3.1. The velocity against physical constraints in converging/diverging channel

The governing physical constraints significantly contribute in the fluid behaviour between convergent/divergent channels. In the particular analysis, these are Re, γ_1 (parameter due to slippery walls) and α (convergent/divergent parameter). The significant impacts of aforesaid constraints on the velocity $F(\eta)$ are furnished in Figures 5 and 6 over the feasible region of the channel. The parallel results are plotted for $[(Al_2O_3\text{-}CuO)/C_2H_6O_2]_{hnf}$ and $[(Al_2O_3\text{-}CuO\text{-}Fe_3O_4)/C_2H_6O_2]_{mhnf}$.

Figure 5a (converging case $\alpha = -5^o$) and 5b (diverging case $\alpha = 5^o$) reveal the behaviour of $[(Al_2O_3\text{-}CuO)/C_2H_6O_2]_{hnf}$ and $[(Al_2O_3\text{-}CuO\text{-}Fe_3O_4)/C_2H_6O_2]_{mhnf}$ by varying Re in convergent and divergent channel, respectively. From Figure 5a, it is examined that the velocity increases by changing Re from 30–180. For $[(Al_2O_3\text{-}CuO)/C_2H_6O_2]_{hnf}$ velocity increases rapidly than $[(Al_2O_3\text{-}CuO\text{-}Fe_3O_4)/C_2H_6O_2]_{mhnf}$. Physical reason behind this behaviour is the densities of both the nanofluids. The addition of Fe_3O_4 in the hybrid nano-additives ($Al_2O_3\text{-}CuO$) enhances the density of $[(Al_2O_3\text{-}CuO\text{-}Fe_3O_4)/C_2H_6O_2]_{mhnf}$ due to which intermolecular forces behave dominantly that resists the fluid motion. The high Re contributed in increase in the velocity $F(\eta)$ in convergent channel.

Physically, the flow rate rises in converging channel and pressure declines due to which the velocity increases because pressure and velocity are in inverse proportion to each other. Figure 5b elaborates the velocity profile in divergent channel against Re within the range variations from 30–180. Physically, flowing area increases in the direction of flow due to divergent channel, the velocity decreases and pressure rises under these circumstances. Therefore, flow rate declines and backflow visualized near the channel walls.

Similarly, Figure 5c and 5d furnishing the behaviour of $[(Al_2O_3\text{-}CuO)/C_2H_6O_2]_{hnf}$ and $[(Al_2O_3\text{-}CuO\text{-}Fe_3O_4)/C_2H_6O_2]_{mhnf}$ against varying α. Physically, area decreases in the direction of flow due to convergent channel due to which flow rate become dominant and pressure drops which allow that the fluid particles move faster. On the other hand, decrement in the fluid movement is observed in Figure 5d due to divergent walls (α positive) because in this direction, flow rate drops and pressure becomes dominant which push the fluid particles along the walls and backflow phenomena occurred.
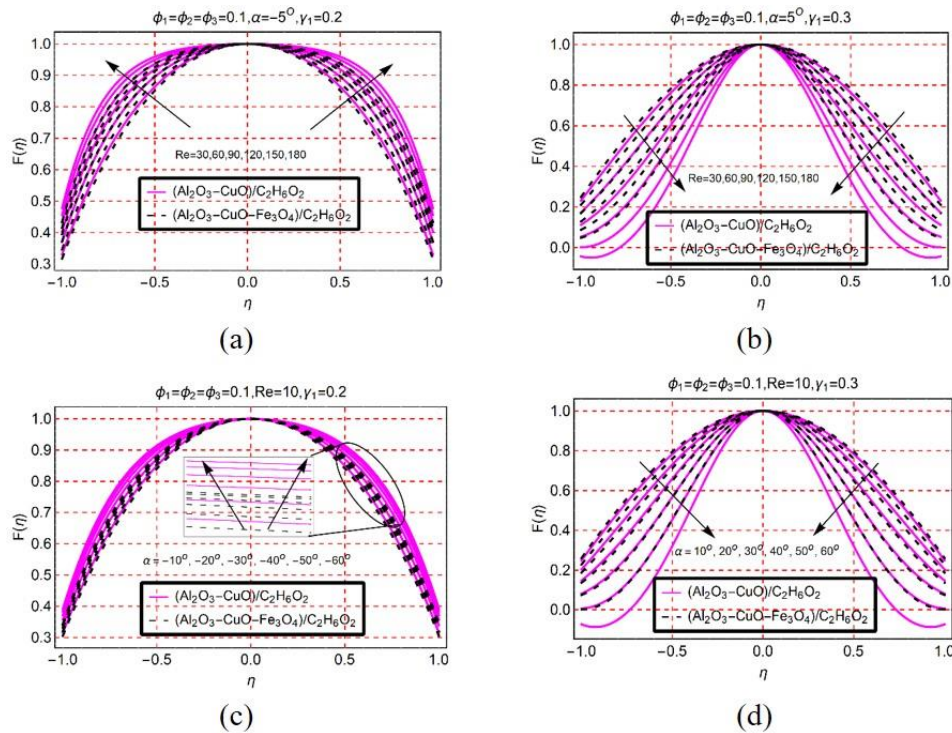
Figure 5. $F(\eta)$ against (a) Re vary convergent (b) Re vary divergent (c) α vary convergent (d) α vary divergent channel.

The influences of γ_1 on the velocity of $[(\mathrm{Al_2O_3\text{-}CuO})/\mathrm{C_2H_6O_2}]_{\text{hnf}}$ and $[(\mathrm{Al_2O_3\text{-}CuO\text{-}Fe_3O_4})/\mathrm{C_2H_6O_2}]_{\text{mhnf}}$ can be visualized in Figure 6a (converging case $\alpha = -5^0$) and Figure 6b (diverging case $\alpha = 5^o$). The upturns in the velocity are examined for both convergent and divergent walls. At the walls, the velocity upturns rapidly because the fluid particles move faster due to imposing slip effects at the walls. The profile is sharp at the central line for diverging channel. Physically, flow rate drops and pressure enhances at the central location of the channel which the particles move at maximum velocity along the middle location of the channel.
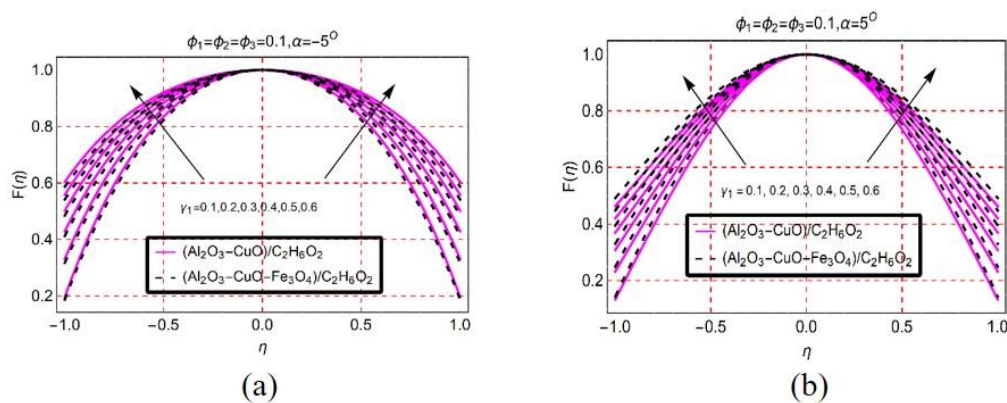

Figure 6. $F(\eta)$ against (a) γ_1 convergent (b) γ_1 divergent channel.

3.2. The Temperature against physical constraints in converging/diverging channel

The dissipation effects are very helpful for thermal enhancement in the study of nanofluids. Therefore, Figure 7a (converging case $\alpha = -5^o$) and 7b (diverging case $\alpha = 5^o$) designed to support the effects of Ec on the temperature of $[(Al_2O_3\text{-}CuO)/C_2H_6O_2]_{hnf}$ and $[(Al_2O_3\text{-}CuO\text{-}Fe_3O_4)/C_2H_6O_2]_{mhnf}$. From the analysis, it is evident that the temperature upsurges by increasing the effects of viscous dissipation. The internal energy of the fluid particles rises due to stronger dissipation effects. However, it is observed that in $[(Al_2O_3\text{-}CuO\text{-}Fe_3O_4)/C_2H_6O_2]_{mhnf}$ has high heat transfer mechanism than $[(Al_2O_3\text{-}CuO)/C_2H_6O_2]_{hnf}$. Physically, tri-hybrid nanoparticles strengthen thermal conductivity of $[(Al_2O_3\text{-}CuO\text{-}Fe_3O_4)/C_2H_6O_2]_{mhnf}$ which allow them to store more heat than binary-hybrid nanomaterial in $[(Al_2O_3\text{-}CuO)/C_2H_6O_2]_{hnf}$. Further, quite rapid increment in the heat transfer is explored in the case of divergent channel.

The temperature trends in $[(Al_2O_3\text{-}CuO)/C_2H_6O_2]_{hnf}$ and $[(Al_2O_3\text{-}CuO\text{-}Fe_3O_4)/C_2H_6O_2]_{mhnf}$ due to opening or narrowing walls in the direction of flow are plotted in Figure 7c and 7d, respectively. It is investigated that for convergent channel the temperature is maximum than in divergent channel. Physically, in convergent channel flow rate rise due to which the frictional force upsurges between the adjacent layers of the fluid and ultimately the fluid temperature rises.
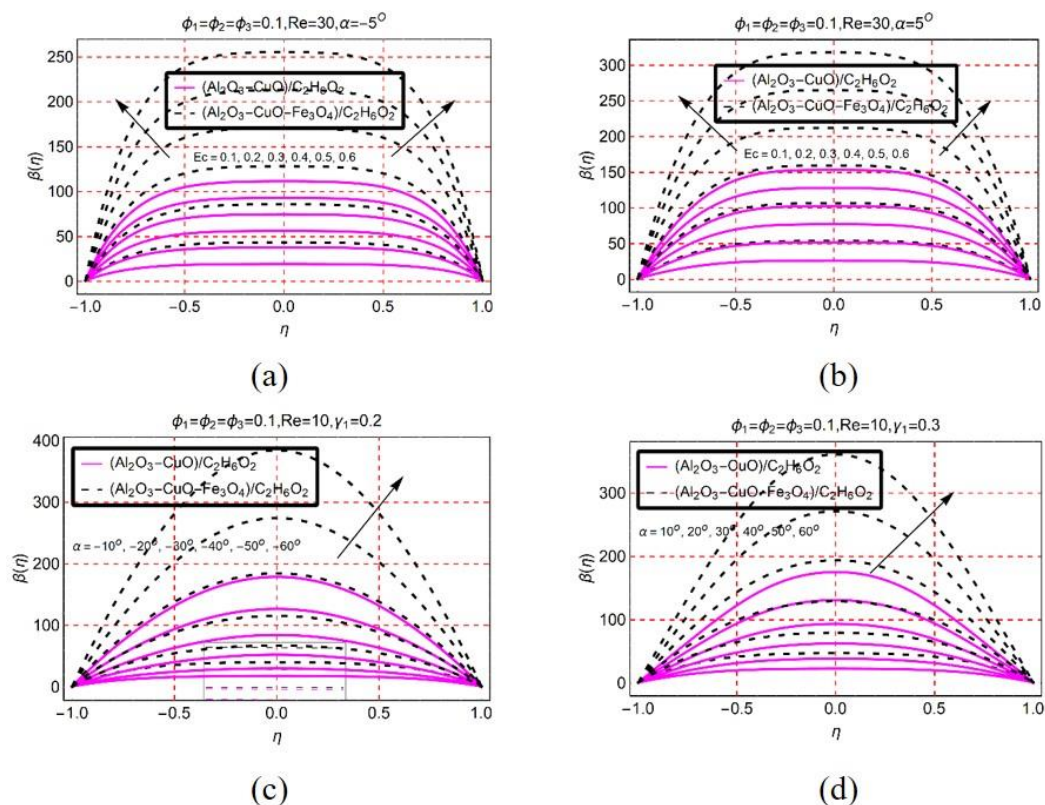

Figure 7. $\beta(\eta)$ via (a) Ec convergent (b) Ec divergent (c) α convergent (d) α convergent.

Figure 8 is the clear description of temperature for $[(Al_2O_3\text{-}CuO)/C_2H_6O_2]_{hnf}$ and $[(Al_2O_3\text{-}CuO\text{-}Fe_3O_4)/C_2H_6O_2]_{mhnf}$ for different Re and velocity slip constraints (γ_1). From these Figures, it is

examined that the temperature drops in convergent channel due to increasing Re and γ_1 values. However, upsurges in the temperature are noted in divergent channel for Re. The temperature is maximum at the mean position of the channel. Ternary hybrid nanofluid has maximum thermal storage ability due to ultra-high thermal conductance than hybrid nanofluid.
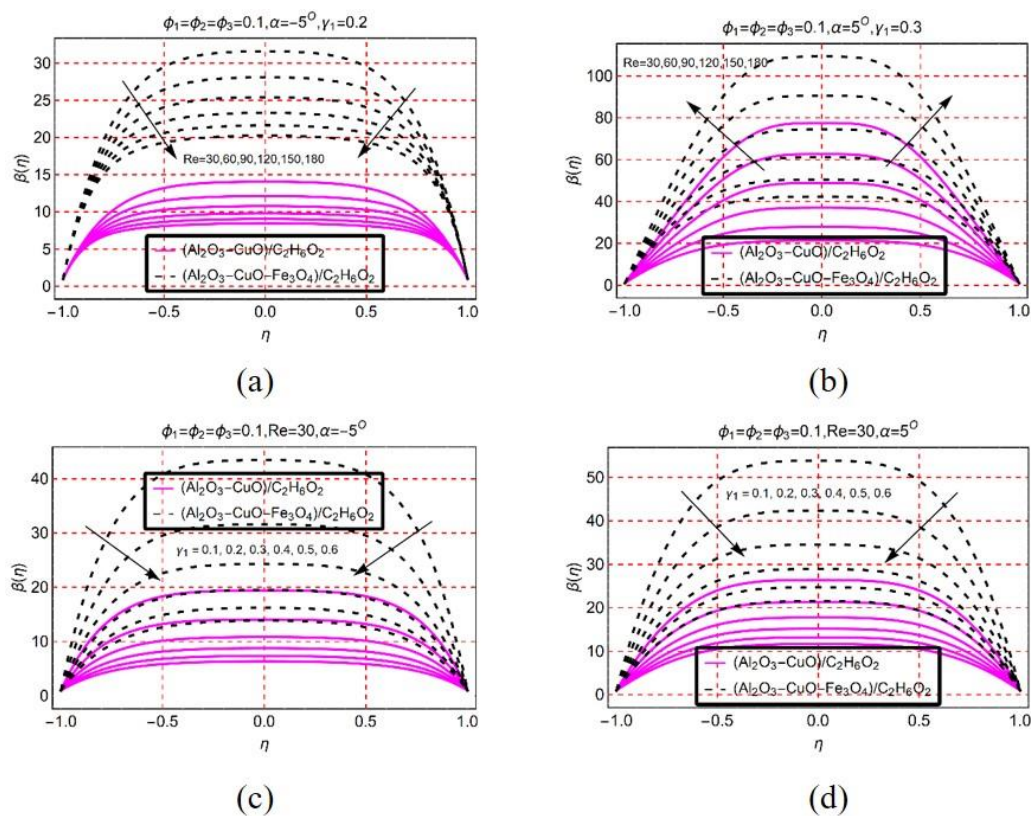

Figure 8. $\beta(\eta)$ via (a) Re convergent (b) Re divergent (c) γ_1 convergent (d) γ_1 divergent.

3.3. Thermophysical attributes against volumetric friction

Comparison of effective properties thermal conductivity, density and viscosity against different nanoparticles concentrations is depicted in Figures 9–11. These results indicate that how effective properties change under various nanoparticles concentration for mono, hybrid and ternary nanofluids. Improved thermal conductivity of ternary nanofluid is very high (due to composite thermal conductivity of trinanoparticles) than hybrid followed by simple nanofluids. This property of ternary nanofluid is better for thermal enhancement and make them effective for industrial applications. Similarly, density and viscosity of ternary nanoliquid is dominant over hybrid and common nanofluids. In hybrid nanofluid, ϕ_2 varies wheraes; fixed ϕ_1, ϕ_2 with changing concentration ϕ_3 taken for ternary nanofluid. Therefore, density, viscosity and thermal conductivity of trinanoparticles jointly contribute in thermal enhancement of ternary fluid.

Further, these results also helpful to predict the concentration factor of nanoparticles to achieve desired amount of heat. The plotted results directly influenced in the fluid motion and temperature of nanofluids and comprehensively discussed in Sections 4.1 and 4.2, respectively.
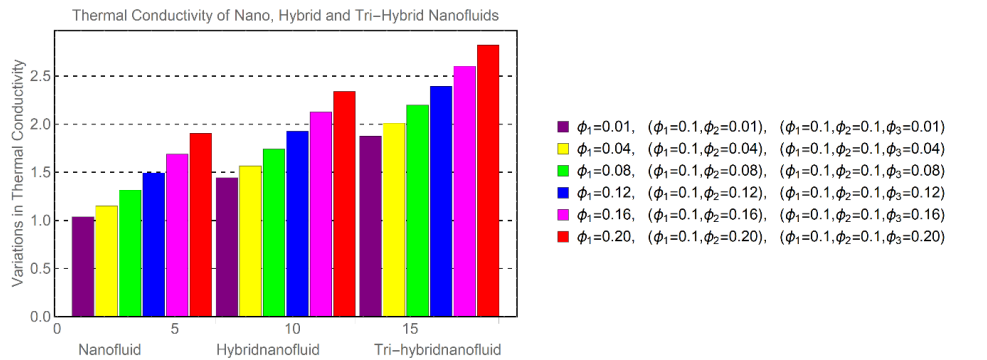
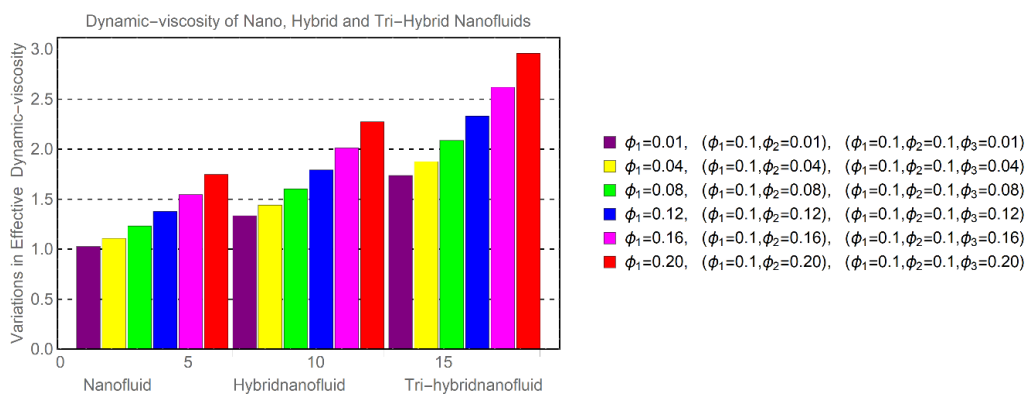**Figure 9.** Thermal conductivity via volumetric fraction.

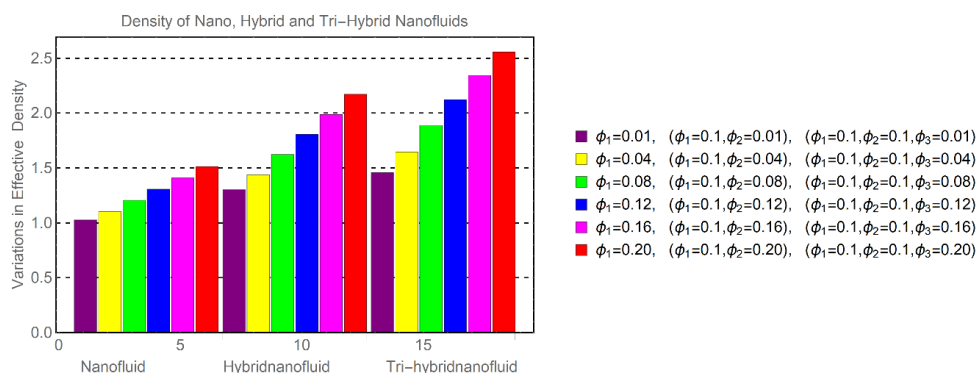**Figure 10.** Dynamic viscosity via volumetric fraction.

Figure 11. Density via volumetric fraction.

3.4. Skin friction coefficient

The trends of shear stresses via Re and γ_1 are furnished in Figure 12 for convergent and divergent channel. From keen survey of the results, it is examined that shear stresses declines by

strengthen Re and slip effects (γ_1). However, maximum decrement is noticed for hybrid nanofluid. The study of walls shear stresses would be beneficial for many industrial and technological purposes.
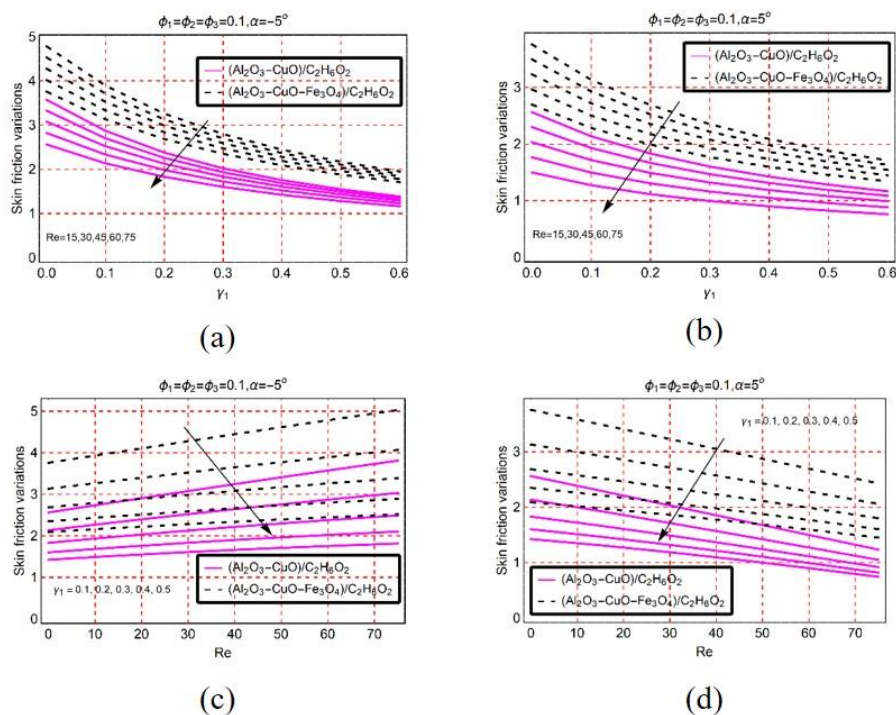

Figure 12. Skin firction via (a) Re convergent (b) Re divergent (c) γ_1 convergent (d) γ_1 divergent.

3.5. Study and code validation

The code and study validation is performed in this section using LSM. The tabulated results (Table 6) show that the computed results for $-F''(0)$ when ϕ_i for $i = 1,2,3$ and γ_1 set as zero are alingned with previously published work. This gives both the study as well as code validation.

Table 6: Present computation and comparison with previously published work for $-F''(0)$.

	Converging walls $\alpha = -5^o$		
Re	Current LSM results	Turkyilmazoglu [29]	Motsa et al. [30]
10	1.78455	1.784547	1.784547
30	1.41369	1.413692	1.413692
50	1.12199	1.121989	1.121989
	Diverging walls $\alpha = 5^o$		
Re	Current LSM results	Turkyilmazoglu [29]	Motsa et al. [30]
20	2.52719	2.527192	2.527192
60	3.94214	3.942140	3.942140
100	5.86917	5.869165	5.869165

4.　Conclusions

The least square analysis of ternary hybrid nanofluid model formulated for slippery converging/diverging channel is conducted and discussed in depth. The core findings of the study are as follows:

- The ternary nanofluid movement declines for diverging case and increasing Re and back flow observed near the walls.
- The slip effects ($\gamma_1 = 0.1, 0.2, 0.3, 0.4, 0.5, 0.6$) on the channel walls are important to increase the velocity of the fluid inside the channel.
- Ternary nanofluid found to be outstanding heat transfer than common hybrid nanofluids and the role composite thermal conductivity of trinanoparticles is significant for this fact.
- In the presence of dissipation effects ($Ec = 0.1, 0.2, 0.3, 0.4, 0.5, 0.6$) significantly boosts the temperature $\beta(\eta)$ in converging channel and is maximum for ternary nanofluid.
- The comparison of thermophysical properties shown that when ϕ_i for $i = 1, 2, 3$ increases from 1% to 20% then density, thermal conductivity and heat capacity of ternary nanofluid is dominant over simple nano and hybrid nanofluids and is directly proportional to the %-volume concentration.
- The validity of study performed for various values of $Re = 10, 30, 50$ for converging case ($\alpha = -5^o$) and $Re = 20, 60, 100$ for diverging case ($\alpha = 5^o$) while keeping other physical parameters fixed and found that the study is aligned with existing science literature.

Acknowledgments

Conflict of interest

There is no financial/competing interest regarding to this work.

References

1. S. U. S. Choi, J. A. Eastman, Enhancing thermal conductivity of fluids with nanoparticles, *ASME*, 1995.
2. R. R. Sahoo, Experimental study on the viscosity of hybrid nanofluid and development of a new correlation, *Heat Mass Transfer*, **56** (2020), 3023–3033. https://doi.org/10.1007/s00231-020-02915-9
3. M. Zayan, A. K. Rasheed, A. John, M. Khalid, A. F. Ismail, Experimental investigation on rheological properties of water based novel ternary hybrid nanofluids, 2021. https://doi.org/10.26434/chemrxiv.13710241
4. E. A. Algehyne, H. F. Alrihieli, M. Bilal, A. Saeed, W. Weera, Numerical approach toward ternary hybrid nanofluid flow using variable diffusion and non-Fourier's concept, *ACS Omega*, **7** (2022), 29380–29390. https://doi.org/10.1021/acsomega.2c03634

5. A. Dezfulizadeh, A. Aghaei, A. H. Joshaghani, M. M. Najafizadeh, An experimental study on dynamic viscosity and thermal conductivity of water-Cu-SiO$_2$-MWCNT ternary hybrid nanofluid and the development of practical correlations, *Powder Technol.*, **389** (2021), 215–234. https://doi.org/10.1016/j.powtec.2021.05.029

6. S. Alshahrani, N. A. Ahammad, M. Bilal, M. E. Ghoneim, A. Ali, M. F. Yassen, et al., Numerical simulation of ternary nanofluid flow with multiple slip and thermal jump conditions, *Front. Energy Res.*, 2022, 1–9. https://doi.org/10.3389/fenrg.2022.967307

7. J. S. Goud, P. Srilatha, R. S. V. Kumar, K. T. Kumar, U. Khan, Z. Raizah, et al., Role of ternary hybrid nanofluid in the thermal distribution of a dovetail fin with the internal generation of heat, *Case Stud. Therm. Eng.*, **35** (2022), 102113. https://doi.org/10.1016/j.csite.2022.102113

8. I. Zahan, R. Nasrin, S. Khatun, Thermal performance of ternary-hybrid nanofluids through a convergent-divergent nozzle using distilled water-ethylene glycol mixtures, *Int. Commun. Heat Mass Transfer*, **137** (2022), 106254. https://doi.org/10.1016/j.icheatmasstransfer.2022.106254

9. M. Sheikhpour, M. Arabi, A. Kasaeian, A. R. Rabei, Z. Taherian, Role of nanofluids in drug delivery and biomedical technology: methods and applications, *Nanotechnol. Sci. Appl.*, **13** (2020), 47–59. https://doi.org/10.2147/NSA.S260374

10. A. Ahmadian, M. Bilal, M. A. Khan, M. I. Asjad, Numerical analysis of thermal conductive hybrid nanofluid flow over the surface of a wavy spinning disk, *Sci. Rep.*, **10** (2020), 18776. https://doi.org/10.1038/s41598-020-75905-w

11. C. Jin, K. Wang, A. Oppong-Gyebi, J. Hu, Application of nanotechnology in cancer diagnosis and therapy-a mini-review, *Int. J. Med. Sci.*, **17** (2020), 2964–2973. https://doi.org/10.7150/ijms.49801

12. Y. Zhang, M. Li, X. Gao, Y. Chen, T. Liu, Nanotechnology in cancer diagnosis: progress, challenges and opportunities, *J. Hematol. Oncol.*, **12** (2019), 137. https://doi.org/10.1186/s13045-019-0833-3

13. A. A. Minea, M. G. Moldoveanu, Overview of hybrid nanofluids development and benefits, *J. Eng. Thermophys.*, **27** (2018), 507–514. https://doi.org/10.1134/S1810232818040124

14. N. A. C. Sidik, I. M. Adamu, M. M. Jamil, G. H. R. Kefayati, R. Mamat, G. Najafi, Recent progress on hybrid nanofluids in heat transfer applications: a comprehensive review, *Int. Commun. Heat Mass Transfer*, **78** (2016), 68–79. https://doi.org/10.1016/j.icheatmasstransfer.2016.08.019

15. H. Adun, D. Kavaz, M. Dagbasi, Review of ternary hybrid nanofluid: synthesis, stability, thermophysical properties, heat transfer applications, and environmental effects, *J. Clean. Prod.*, **328** (2021), 129525. https://doi.org/10.1016/j.jclepro.2021.129525

16. H. Adun, M. Mukhtar, M. Adedeji, T. Agwa, K. H. Ibrahim, O. Bamisile, et al., Synthesis and application of ternary nanofluid for photovoltaic-thermal system: comparative analysis of energy and exergy performance with single and hybrid nanofluids, *Energies*, **14** (2021), 4434. https://doi.org/10.3390/en14154434

17. N. A. S. Muzaidi, M. A. Fikri, K. N. S. W. S. Wong, A. Z. M. Sofi, R. Mamat, N. M. Adenam, et al., Heat absorption properties of CuO/TiO$_2$/SiO$_2$ trihybrid nanofluids and its potential future direction towards solar thermal applications, *Arab. J. Chem.*, **14** (2021), 103059. https://doi.org/10.1016/j.arabjc.2021.103059

18. A. I. Ramadhan, W. H. Azmi, R. Mamat, Experimental investigation of thermo-physical properties of tri-hybrid nanoparticles in water-ethylene glycol mixture, *Walailak Journal of Science and Technology*, **18** (2021), 9335. https://doi.org/10.48048/wjst.2021.9335

19. G. Li, J. Wang, H. Zheng, G. Xie, B. Sundén, Improvement of cooling performance of hybrid nanofluids in a heated pipe applying annular magnets, *J. Therm. Anal. Calorim.*, **147** (2021), 4731–4749. https://doi.org/10.1007/s10973-021-10848-6

20. N. A. Zainal, R. Nazar, K. Naganthran, I. Pop, MHD flow and heat transfer of hybrid nanofluid over a permeable moving surface in the presence of thermal radiation, *Int. J. Numer. Method. Heat Fluid Flow*, **31** (2020), 858–879. https://doi.org/10.1108/HFF-03-2020-0126

21. S. Masood, M. Farooq, A. Anjum, Influence of heat generation/absorption and stagnation point on polystyrene–TiO_2/H_2O hybrid nanofluid flow, *Sci. Rep.*, **11** (2021), 22381. https://doi.org/10.1038/s41598-021-01747-9

22. S. Murthy, P. Effiong, C. C. Fei, Metal oxide nanoparticles in biomedical applications, In: *Metal oxide powder technologies*, Elsevier, 2020, 233–251. https://doi.org/10.1016/B978-0-12-817505-7.00011-7

23. N. Ahmed, Adnan, U. Khan, S. T. Mohyud-Din, R. Manzoor, Influence of viscous dissipation on a copper oxide nanofluid in an oblique channel: Implementation of the KKL model, *Eur. Phys. J. Plus*, **132** (2017), 237. https://doi.org/10.1140/epjp/i2017-11504-y

24. A. Shahzad, F. Liaqat, Z. Ellahi, M. Sohail, M. Ayub, M. R. Ali, Thin film flow and heat transfer of Cu-nanofluids with slip and convective boundary condition over a stretching sheet, *Sci. Rep.*, **12** (2022), 14254. https://doi.org/10.1038/s41598-022-18049-3

25. N. S. Khashi'ie, N. M. Arifin, M. Sheremet, I. Pop, Shape factor effect of radiative Cu-Al_2O_3/H_2O hybrid nanofluid flow towards an EMHD plate, *Case Stud. Therm. Eng.*, **26** (2021), 101199. https://doi.org/10.1016/j.csite.2021.101199

26. M. Arif, P. Kimam, W. Kumam, Z. Mostafa, Heat transfer analysis of radiator using different shaped nanoparticles water-based ternary hybrid nanofluid with applications: a fractional model, *Case Stud. Therm. Eng.*, **31** (2022), 101837. https://doi.org/10.1016/j.csite.2022.101837

27. Adnan, U. Khan, N. Ahmed, S. T. Mohyud-Din, D. Baleanu, K. S. Nisar, et al., Second law analysis of magneto radiative GO-MoS_2/H_2O–$(CH_2OH)_2$ hybrid nanofluid, *Comput. Mater. Con.*, **68** (2021), 213–228. https://doi.org/10.32604/cmc.2021.014383

28. P. Gumber, M. Yaseen, S. K. Rawat, M. Kumar, Heat transfer in micropolar hybrid nanofluid flow past a vertical plate in the presence of thermal radiation and suction/injection effects, *Partial Differential Equations in Applied Mathematics*, **5** (2022), 100240. https://doi.org/10.1016/j.padiff.2021.100240

29. M. Turkyilmazoglu, Extending the traditional Jeffery-Hamel flow to stretchable convergent/divergent channels, *Computers & Fluids*, **100** (2014), 196–203. https://doi.org/10.1016/j.compfluid.2014.05.016

30. S. S. Motsa, P. Sibanda, G. Marewo, On a new analytical method for flow between two inclined walls, *Numer. Algor.*, **61** (2012), 499–514. https://doi.org/10.1007/s11075-012-9545-2